Smart Hybrid Materials Equipped by Nanoreservoirs of Therapeutics

Carlos Mendoza-Palomares,[†,‡,#] Alice Ferrand,[†,§,#] Sybille Facca,[†,#] Florence Fioretti,[†,‡,#] Guy Ladam,[⊥,#] Sabine Kuchler-Bopp,[†,‡] Thomas Regnier,[¶] Didier Mainard,[▽] and Nadia Benkirane-Jessel[†,▽,*]

[†]Institut National de la Santé et de la Recherche Médicale (INSERM), Unité 977, 11 rue Humann, 67085 Strasbourg, France, [‡]Université de Strasbourg, Faculté de Chirurgie Dentaire, 1 place de l'Hôpital, 67000 Strasbourg, France, [§]LIPHT (UMR 7165 CNRS), ECPM, 25 rue Becquerel, 67087 Strasbourg, France, [⊥]La2B (Laboratoire de Biophysique et Biomatériaux), EA 3233, Université de Rouen, Centre Universitaire d'Evreux, 1 rue du 7ème Chasseurs, 27002 Evreux, France, [¶]IBMM (UMR 5247 CNRS), Université Montpellier 1&2, Cap Alpha, avenue de l'Europe, Clapiers, 34940 Montpellier, France, and [▽]Hôpital Central, Service de Chirurgie Orthopédique and UMR 7561 CNRS, 29 avenue du Maréchal de Lattre de Tassigny, 54035 Nancy, France [#]These authors equally contributed to this work.

ABSTRACT

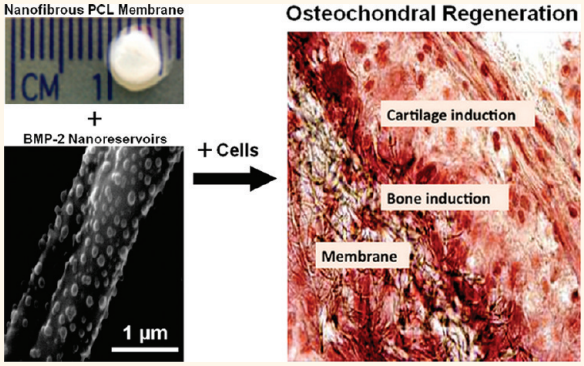

Nanobiotechnology enables the emergence of entirely new classes of bioactive devices intended for targeted intracellular delivery for more efficacies and less toxicities. Among organic and inorganic approaches currently developed, controlled release from polymer matrices promises utmost clinical impact. Here, a unique nanotechnology strategy is used to entrap, protect, and stabilize therapeutic agents into polymer coatings acting as nanoreservoirs enrobing nanofibers of implantable membranes. Upon contact with cells, therapeutic agents become available through enzymatic degradation of the nanoreservoirs. As cells grow, divide, and infiltrate deeper into the porous membrane, they trigger slow and progressive release of therapeutic agents that, in turn, stimulate further cell proliferation. This constitutes the first instance of a smart living nanostructured hybrid membrane for regenerative medicine. The cell contact-dependent bioerodable nanoreservoirs described here will permit sustained release of drugs, genes, growth factors, *etc.*, opening a general route to the design of sophisticated cell-therapy implants capable of robust and durable regeneration of a broad variety of tissues.

KEYWORDS: biomineralization · biomaterials · osteochondral regeneration · drug delivery · nanostructured coatings · nanoreservoirs of active molecules

Smart nanoengineered materials allow novel therapeutic modalities such as improved specific cell targeting by means of nanoparticle-based drugs, resulting in decreased side effects for patients. Other advances are being made in sophisticated biomaterials for use in less invasive surgical implantations, leading to shorter recovery times and decreased risk of postoperative infections or other complications. Such innovations will improve the quality of life, extend life expectancies, and should reduce the overall cost of healthcare. Biomaterials play central roles in modern strategies in regenerative medicine and tissue engineering as designable biophysical and biochemical milieus that direct cellular behavior and function.

Tissue engineering is an interdisciplinary field that has attempted to implement a variety of processing methods for synthetic and natural polymers to fabricate tissues and organs regeneration scaffolds. The study of structure–function relationships in both normal and pathological tissues has been coupled with the development of biologically active substitutes or engineered materials. The guidance provided by biomaterials may facilitate restoration of structure and function of damaged or dysfunctional tissues. Such materials should provide provisional 3-D support to interact with cells in ways that control their function, by guiding the spatially and temporally complex multicellular processes of tissue formation and regeneration.[1−9]

Our expected outcomes are the development of clinical applications in the field of tissue engineering and nanomedicine, and more particularly in bone and cartilage regeneration. Recently, our group has focused on the development of nanostructured active biomaterials within this field. With the aging of the population and a correlated increase in the incidence of osteo-articular damage, great attention is focused on tissue engineering solutions to restore durable articular function and comfort. This is considered a highly accessible first target for regenerative medicine due to the nature of tissues concerned. Current methods aim at repairing

* Address correspondence to nadia.jessel@inserm.fr.

Received for review October 5, 2011 and accepted December 17, 2011.

Published online December 18, 2011
10.1021/nn203817t

full-thickness cartilage defects.[10,11] These limited techniques are generally not sufficient to ensure durable cartilage repair, and it is becoming apparent that without a healthy subchondral bed, the entire osteochondral unit is likely to fail. Therefore, the future of articular cartilage repair depends on the development of advanced implants allowing entire osteochondral unit replacement, not only bone or cartilage regeneration as addressed until now. We report here the first demonstration of bone and cartilage regeneration by implementing a novel strategy based on a synthetic nanoengineered biomimicking membrane functionalized with nanoreservoirs of a growth factor (bone morphogenetic protein 2, BMP-2).

Several biomimicking medical devices for regenerative medicine have been inspired from the intricate fibrillar architecture of natural extra-cellular matrix (ECM) components. Such matrices have already shown remarkable success in tissue engineering applications, such as reconstruction of a dog urinary bladder,[12] or regeneration after brain injury in a mouse stroke model.[13] However, it is established that inert ECM mimetic scaffolds are not efficient to generate durable tissue repair. Therefore, there is a need for materials ensuring the sustained release of active compounds. To this end, recent advances in nanotechnology have led to various engineered ECM analogues and active biomaterials incorporating drugs, genes, or growth factors within the form of coatings.[14−28]

To date, three polymer processing technologies (self-assembly, phase separation, electrospinning) allow the fabrication of nanofibrous scaffolds.[29−32] Electrospinning allows fiber formation down to the 10-nm scale.[33] Our strategy for regenerating the osteochondral unit combines a synthetic electrospun nanofibrous membrane (ENM) comprising the FDA-approved poly(ε-caprolactone) (PCL) polymer, and the bioactive growth factor BMP-2 entrapped into polymer nanoreservoirs (NR) built atop the nanofibers according to the layer-by-layer technology.[7,15−24] This is the first investigation of combined biodegradable PCL and active molecules for regenerative medicine.

The European and American authorities have already approved the use of BMP-2 for bone regeneration applications. For example, Medtronics offers InductOS which is a basic collagen matrix (of animal origin) soaked in BMP-2 (12 mg). The efficacy of this kind of combination device is dependent on slow release kinetics of BMPs. This criterion is recognized as the critical, most challenging requirement for combination implants. For efficient bone regeneration, the target cells require a reliable and continuous exposure to growth factors over an extended period of time, until the induction of new bone or subchondral bone. The currently available devices are totally unsophisticated in this respect. In contrast, our innovative medical device, with cell contact-dependent delivery from nanoreservoirs, is designed specifically for reliable and sustained availability of BMP-2. This strategy aims at a dramatic enhancement of therapeutic efficacy at reduced cost.

RESULTS AND DISCUSSION

From the nanostructured organization surrounding the nanofibers, we can observe the effective step-by-step buildup of the active nanoreservoirs achieved by simple alternate immersions into a polycation (dendrigraft poly(L-lysine), DGL) solution and the therapeutic agent (BMP-2) solution (Figures 1A−E). The buildup of the nanoreservoirs embedding BMP-2 was followed by quartz crystal microbalance (QCM-D), revealing linear growth in the wet adsorbed mass and the hydrodynamic thickness, and confirming the nanometric scale of the nanoreservoirs (Figure 1F). Each BMP-2 injection step resulted in the immobilization of about 180 ng cm^{-2} BMP-2 up to the NR_3 architecture, and about 330 ng cm^{-2} for further steps (Figure 1G). This difference is not unexpected considering that a few adsorption steps are generally required to overcome the possible influence of the underlying substrate and, in turn, to reach a steady layer-by-layer growth regime.[35] We additionally showed the versatility of the deposition method by applying it successfully to that already used in the clinic BioGide collagen membranes (Geistlich) (Figure 2).

The capacity of nanoreservoirs to induce *in vitro* specific gene expression by human osteoblasts was verified by immunochemistry after 7 days of culture (Figure 3A). Treated ENM membranes enhanced the proliferation of human osteoblasts *in vitro* (Figure 3B), while specific gene expression after 7-day culture was fostered by NR_3 architectures: 43.7 ($\pm$8.8)-fold higher osteocalcin gene expression compared to cells grown onto nonfunctionalized NR_0 membranes (Figure 3C), 135.3 ($\pm$27.5)-fold higher bone sialoprotein (BspII) gene expression (major structural protein of bone matrix), and 186.2 ($\pm$50.1)-fold higher osteopontin gene expression. For tissue engineering application, we tested these nanostructured membranes as platforms to differentiate stem cells and generate active tissue. To this end, treated ENM membranes were seeded with embryonic stem cells and their potentiality to induce bone formation *in vivo* was confirmed by the expression of osteopontin after 30 days of implantation in mice (Figure 3D).

To analyze more deeply the capacity of these membranes to induce bone mineralization, an ENM NR_3 membrane was inspected by confocal Raman microspectroscopy after 21-day *in vitro* mineralization by human osteoblasts, to detect calcium phosphate (CaP) deposition. A nonmineralized ENM NR_3 membrane was analyzed as a reference. Raman signatures are very similar (Figure 4A), except in the region around 960 cm^{-1} relative to CaP, where the signatures of the

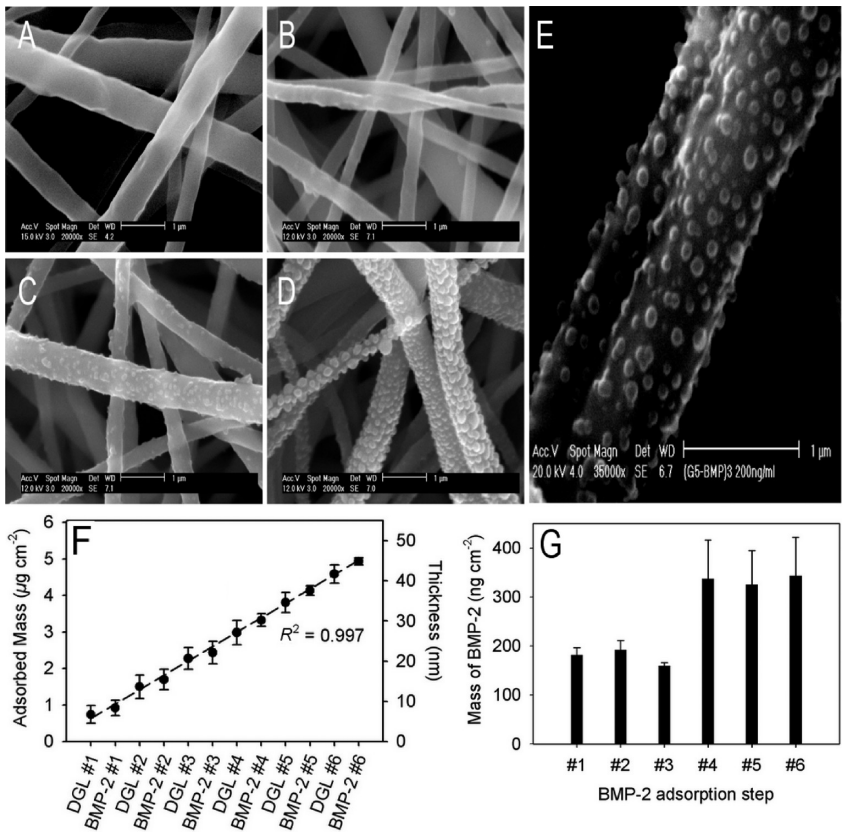

Figure 1. (A–D) SEM images (×20.000) of ENM membranes showing the layer-by-layer deposition of NR_n nanoreservoirs incorporating BMP-2. (A) NR_0; (B) NR_1; (C) NR_3; (D) NR_6. (E) Zoomed SEM image of C (×35.000). Scale bars: 1 μm. (F) Evolution of the mean wet mass and hydrodynamic thickness during the buildup of NR_6 nanoarchitectures onto gold-coated quartz sensors followed by quartz crystal microbalance (QCM-D). The normalized frequency curves ($\Delta f_n/n$) of the different overtones were almost superimposed (data not shown), meaning that the deposits were rigid enough to allow the application of the Sauerbrey relation.[34,35] Mass and thickness values were derived from the 3rd overtone frequency changes. Error bars represent the standard errors over two distinct experiments. The dotted line represents the linear regression fit accompanied by the corresponding determination coefficient R^2. (G) Mean wet mass increments upon successive BMP-2 deposition steps derived from the data shown in panel F.

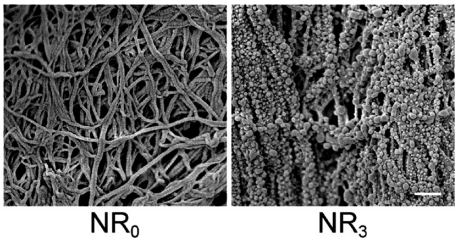

Figure 2. SEM visualization of the collagen membrane already used in the clinic (BioGide, Geistlich) before and after BMP-2 nanoreservoirs formation. Scale bar: 1 μm.

mineralized membrane show a significant peak proving the presence of CaP, contrary to the unmineralized membrane. Raman signatures of the latter display a weak peak at 963 cm^{-1} relative to PCL, whose contribution to the CaP peak on mineralized membranes is negligible.[36] A 2-D mapping of the CaP peak intensity over the mineralized membrane (Figure 4B), reveals a massive CaP deposition all over the ENM NR_3 membrane. The peaks at 960 cm^{-1} and 430 cm^{-1} (Figure 4A) reveal the presence of hydroxyapatite (HAp) and/or octacalcium phosphate (OCP), while the peak at 1005 cm^{-1} is unambiguously attributable to OCP.[37,38] If the coating was pure OCP, a shoulder should be present at 966–970 cm^{-1}.[37,38] The absence of such a feature is necessarily due to the overwhelming contribution of the HAp peak, which indirectly confirms the coexistence of HAp and OCP. The presence of OCP is not surprising as it is a precursor phase of HAp in bone.[38]

The set of results described above is highly promising in view of bone induction, and points to potentially far more efficient surgical approaches than are currently available. To this end, we propose an ENM-based medical device (Implant Type 1 "NanoM1") for small lesions of bone without the need of osteoblasts from patients (Figure 5). In addition, we propose an Implant Type 2 ("NanoM1C"), consisting of a NanoM1 device supplemented with cells (osteoblasts and/or chondrocytes) from the patients (Figure 6), in order to address larger bone and/or cartilage lesions. We have the final products ready to use for preclinical trials, for bone regeneration in maxillofacial and orthopedic

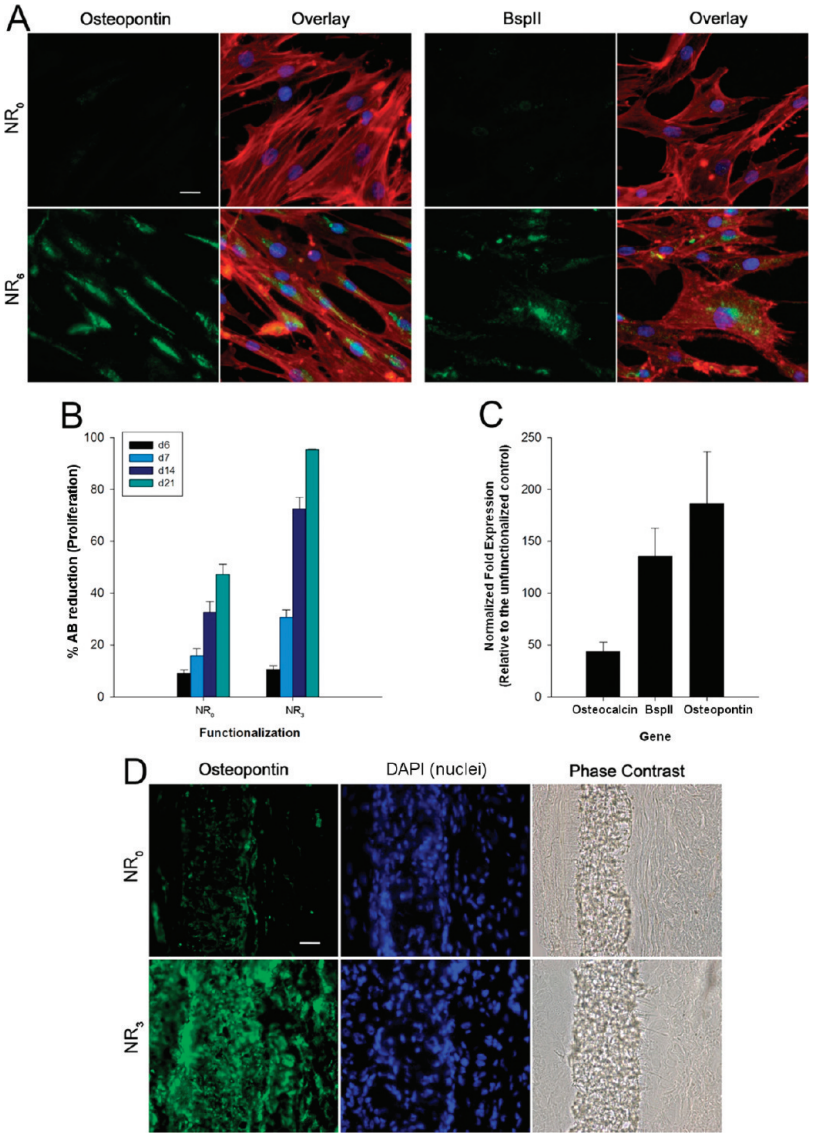

Figure 3. (A) Osteopontin and BspII expression in human osteoblasts after 7 days of culture onto pristine ENM NR_0 and ENM NR_6 membranes. Green, osteopontin and BspII expression; red, phalloidin staining for actin cytoskeleton; blue, DAPI staining for the nucleus. Scale bar: 20 μm. (B) *In vitro* proliferation of human osteoblasts growing on the surface of ENM NR_3 membranes. (C) Differences in gene expression monitored by qPCR of bone markers in human osteoblasts after 7 days of culture onto ENM NR_3 membranes as compared with nonfunctionalized ENM NR_0 membranes. (D) *In vivo* osteopontin expression on ENM NR_3 membranes seeded by stem cells prior to implantation into nude mice for 30 days. Scale bar: 20 μm.

fields, and for osteochondral repair (bone-cartilage unit regeneration), respectively. All implants were used *in vivo* (mouse model), and were found to promote bone and/or cartilage regeneration. Our results clearly indicate colonization of ENM membranes by osteoblasts, as well as mineralization and cartilage regeneration (Figure 6R).

After 2 months of implantation on nude mice (males, 16 week-old), nanomechanical analysis of the retrieved implants showed an increased elastic modulus (2.19 $\pm$ 0.39 GPa) for the Implant Type 1 NanoM1 device in comparison with the ENM NR_0 membrane (1.74 $\pm$ 0.65 GPa), which is likely due to the effect of the incorporated BMP-2. Promisingly, the highest value of elastic modulus was measured for an Implant Type 2 membrane enriched with hOsteoblasts (14.26 $\pm$ 2.16 GPa).

The treatment goal for large chondral or osteochondral defects should be to restore the physiological properties of the entire osteochondral unit, aiming to achieve a more predictable repair tissue that closely resembles the native articular surface and remains durable over time. We report here the first demonstration of subchondral bone regeneration using a strategy based on a synthetic nanoengineered electrospun membrane manufactured using an FDA-approved polymer and functionalized with nanoreservoirs of a growth factor (BMP-2). At this step, our results show that we can (i) design an ENM implant controlled in size and thickness, enriched in BMP-2 (Implant Type 1) and,

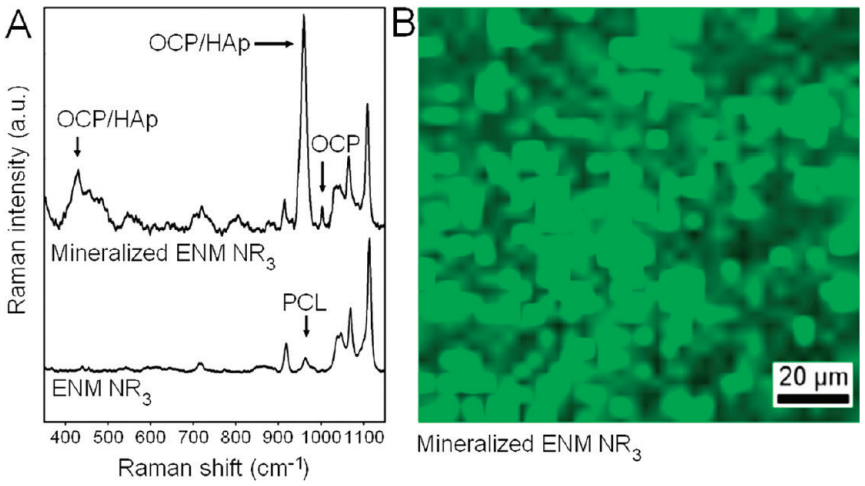

Figure 4. (A) Typical Raman spectra of (down) a native and (up) a mineralized ENM NR_3 membrane (HAp, hydroxyapatite; OCP, octacalcium phosphate). Mineralization was performed by 21-day incubation of the membrane with human osteoblasts in adequate medium. The spectra are offset for sake of clarity. (B) 2-D mapping of the calcium phosphate peak over the mineralized membrane (100 × 100 μm^2; meshsize 2.8 μm).

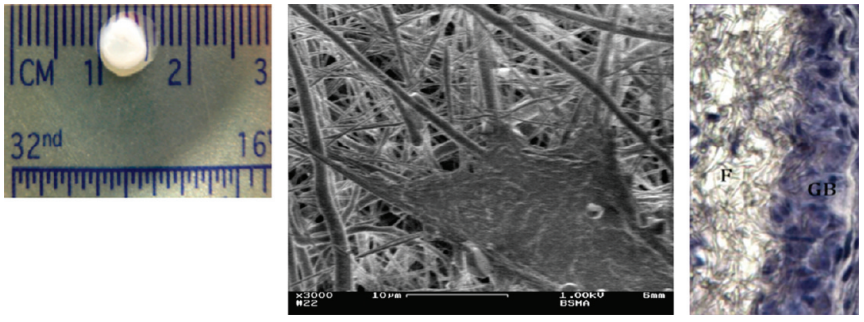

Figure 5. (Left) Implant Type 1 (NanoM1: PCL ENM NR_3). ENM membranes of different sizes and thicknesses can be produced. (Middle) Morphology of osteoblasts on NanoM1 implant after 1 day. Cells are well spread and migrate along nanofibers. (Right) Hematoxylin Eosin staining showing the membrane fibers (F) and generated bone (GB) after implantation of the proposed medical device NanoM1 (*in vivo* in nude mice).

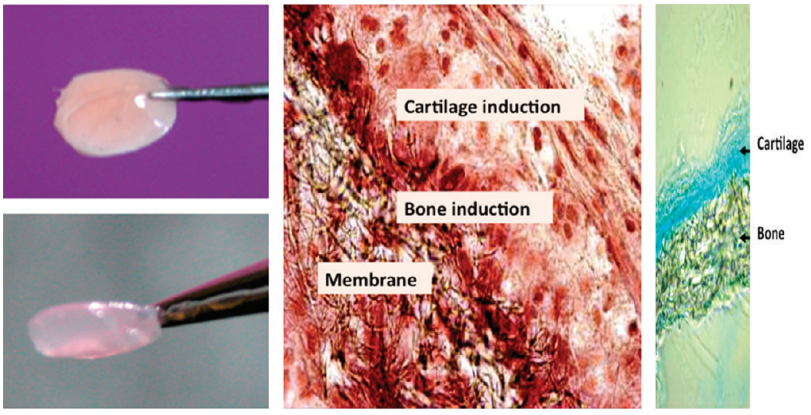

Figure 6. (Left) Implant Type 2 based on the Implant Type 1 supplemented with osteoblasts and chondrocytes from patients for bone-cartilage unit regeneration. (Middle and Right) Osteochondral unit regeneration by Implant Type 2 with osteoblast and chondrocytes as observed after 2 months of implantation into nude mice (right, proteoglycans secreted by chondrocytes were stained with Alcian blue for cartilage induction).

(ii) induce bone formation *in vitro* and *in vivo*. This membrane implant could be used for small lesions of bone without any need to add cells from patients. For large and deep lesions it becomes necessary to seed the implant with osteoblasts from the patient. In the clinic today, surgeons use collagen membranes of animal origin that slowly induce bone formation, but cannot be used for all types of lesion. In this study, we have

deposited human osteoblasts and chondrocytes on the membrane (Implant Type 1) to fabricate a nanostructured active living membrane (Implant Type 2 = Implant Type 1 + osteoblasts + chondrocytes) and have shown bone and cartilage induction. We have also shown that active membranes (enriched in BMP-2) seeded with embryonic stem cells could induce bone regeneration (Figure 3D).

CONCLUSIONS

The innovative medical device described here fulfills and exceeds the criteria for a BMP-2-loaded combination implant; BMP-2 from the nanoreservoirs becomes available in a reliable and sustained cell contact-dependent manner. Degradation of BMP-2 occurs rapidly in aqueous solution. With current systems using collagen matrices soaked with the growth factor, this problem is addressed by overdosing, which may induce adverse side effects. The novelty of our approach lies in the nanoimmobilization and the protection of BMP-2. The nanostructured membrane is produced using a special coating process that entraps the growth factor into nanoreservoirs atop the membrane fibers. Recently, we have elucidated the mechanism by which cells come in contact and interact with such a nanostructured coating.[18,21,24,25] Encapsulated by polymers, BMP-2 is protected and stabilized. Once cells come into contact with nanoreservoirs, cellular enzymes degrade their polymer coating and BMP-2 becomes available. As cells grow, divide, and infiltrate deeper into the porous structure of the membrane they provoke a slow and progressive release of BMP-2 that, in turn, stimulates further proliferation of the cells. This strategy should allow the fabrication of a combination cell-therapy implant capable of robust and durable cartilage repair in large defects. We mention that the possibility to continue the buildup of nanoreservoirs beyond the NR_3 architecture (Figure 1F,G), illustrates the robustness and the versatility of the method: if required by given applications, the method will allow to tune the biological activity or kinetics of action of the implants by varying the NR_n architecture. We believe that our results make a significant contribution to the area of regenerative nanomedicine. The concepts discovered here may serve to design sophisticated implants for placement into a broad variety of tissues.

METHODS

Chemicals. Poly(ε-caprolactone) (PCL), analytical grade, was purchased from Sigma-Aldrich. PCL was dissolved in a mixture of dichloromethane/dimethylformamide (DCM/DMF 50/50 vol/vol) at 15% wt/vol and was stirred overnight before use. The dendri-graft poly(L-lysine) (DGL) was purchased from Colcom (Montpellier, France). In this study, we have used the fifth-generation DGL^{G5}. Human recombinant BMP-2 was purchased from PeproTech. Sodium alginate medium viscosity was from Sigma, and hyaluronic acid (MW 132.300) was from Lifecore. Rat-tail type I collagen was purchased from Institut de Biotechnologies Jacques Boy.

Electrospinning. A homemade standard electrospinning setup was used to fabricate the PCL scaffolds. The PCL solution was poured into a 5 mL syringe and ejected through a needle with a diameter of 0.5 mm at a flow rate of 1.2 mL h^{-1}, thanks to a programmable pump (Harvard Apparatus). A high-voltage power supply (Spellman SL30P10) was used to set 15 kV at the needle. Aluminum foils (20 × 20 cm^2), connected to the ground at a distance from the needle of 17 cm, were used to collect the electrospun PCL scaffold.

SEM Observation. For morphological study, the PCL scaffolds were gold-coated (Edwards Sputter Coater) and observed with a Philips XL-30 ESEM scanning electron microscope in conventional mode (high vacuum) with a Thornley–Everhart secondary electron detector. Cells interactions with electrospun membranes were analyzed by SEM. Cell-seeded samples were fixed with 3% glutaraldehyde for 30 min at 4 °C, gently washed 3 times with PBS, gradually dehydrated with 20%, 40%, 80%, and 100% ethanol each for 5 min, covered with hexamethyldisilazane (HMDS), and finally left to dry overnight in a fumehood. The samples were then imaged using a field effect gun digital scanning electron microscope (FE-SEM, DSM 982 Gemini from LEO) operating at 1 kV.

Buildup of the Nanoreservoirs (NR). For all biological activity experiments, nanoreservoirs (NR) constituted by $(DGL^{G5}/BMP\text{-}2)_n$ layer-by-layer (LbL) architectures were built up onto electrospun PCL membranes by alternating immersion during 15 min in the adequate solutions (300 μL) at the respective concentrations of 50 μM for DGL^{G5} and 200 nM of BMP-2 in the presence of 0.04 M MES and 0.15 M NaCl at pH 5.5. After each deposition step the membranes were rinsed during 15 min with 0.04 M MES and 0.15 M NaCl at pH 5.5. All membranes were sterilized for 30 min by exposure to UV light (254 nm, 30 W, distance 20 cm), and equilibrated in contact with 1 mL of serum-free medium prior to cell culture.

Quartz Crystal Microbalance with Dissipation Monitoring (QCM-D). QCM-D was operated with a D300 system (Q-Sense, Sweden) using a QAFC302 flow chamber and QSX301 gold-coated quartz crystal sensors. This technique consists of measuring the resonance frequency shifts Δf_n and the dissipation factor changes ΔD_n of the quartz crystal sensor upon material deposition, for the fundamental (n = 1), third (n = 3), fifth (n = 5), and seventh (n = 7) overtones.[39] The LbL buildup was performed by successive 5-min injections of DGL^{G5} (50 μg mL^{-1}) and BMP-2 (200 ng mL^{-1}) solutions and rinsing solution (0.04 M MES, 0.15 M NaCl, pH 5.5) through the flow chamber, and monitored *in situ*. A shift Δf_n can be associated, in a first approximation, to the adsorded mass through the Sauerbrey relation:[34] $m = -C \times \Delta f_n/n$, where C is a constant characteristic of the crystal used (C = 17.7 ng cm^{-2} Hz^{-1}). Thicknesses were derived from mass values assuming a film density of 1.1 g cm^{-3}.[35]

Cells Culture. Human primary osteoblasts were obtained from Cell Applications and cultured in Dulbecco's modified Eagle's medium (D-MEM) containing 50 U mL^{-1} penicillin, 50 μg mL^{-1} streptomycin, 2.5 μg mL^{-1} Amphotericin B, and 10% FBS (Life Technologies, Paisley, UK). Cells were incubated at 37 °C in a humidified atmosphere of 5% CO_2. When cells reached subconfluence, they were harvested with trypsin and subcultured.

Confocal Raman Microspectroscopy. Two PCL electrospun membranes were coated with NR_3 nanoreservoirs. One membrane was stored in the buildup medium, while the other was seeded with human osteoblasts and incubated for 21 days in mineralization medium, then fixed with 4% PFA for 2 h, rinsed with PBS, and finally stored in water. The same mineralization treatment was applied to a native membrane as a reference. The membranes were laid upon a glass substrate and dried under a gentle flow of argon prior to analysis by confocal Raman microspectroscopy. Raman measurements were carried out in

air by using a confocal Raman microspectrometer composed of a Raman spectrometer (LabRam HR by Jobin-Yvon Horiba with a 600 lines mm^{-1} grating) coupled to a microscope (model BX41, Olympus) with *xyz* mapping stage *via* optical fibers. The excitation of Raman scattering was operated with a helium−neon laser at a wavelength of 632.8 nm. The laser beam was focused on the sample by means of a ×50LWD microscope objective. A confocal pinhole of 400 μm diameter placed before the entrance slit was used to reject the Raman signal from out-of-focus planes. Raman spectra with good signal-to-noise ratios were recorded with an integration time of 60 s for single spectra and 15 s for 2-D mappings.

Implants Preparation. A sample portion of 5×10^4 human osteoblasts was seeded and incubated for 72 h prior to gel preparation. For the collagen lattices preparation, 3 mL of Rat Tail Type-I Collagen (Institut de Biotechnologies Jacques Boy) were mixed with 5.5 mL of medium containing 10% FBS, 0.5 mL of a 0.1 M NaOH solution, and 1 mL of cell suspension at 2×10^5 cells mL^{-1}. A 0.5 mL portion of the cells suspension was laid on the electrospun membrane and incubated at 37 °C. After 30 min, 0.5 mL of a human chondrocyte suspension (1×10^5 cells mL^{-1}) in an alginate/hyaluronic acid solution (4:1) prepared in 0.15 M NaCl, pH 7.4 were added in order to obtain the 3-layered construct. Cylinders of 5 or 2 mm were cut using a sterile biopsy punch and incubated o/n at 37 °C in a humidified atmosphere of 5% CO_2 prior to *in vivo* experiments (subcutaneous or calvaria).

Cell Proliferation. AlamarBlue (Serotec) was used to assess cellular proliferation. The Alamar Blue test is a nontoxic, water-soluble, colorimetric redox indicator that changes color in response to cell metabolism. In this study, 2×10^4 human osteoblasts were seeded on top of LbL-coated 14 mm-diameter membranes ($n = 3$) placed on 24-well plates. After 6, 7, 14, or 21 days of culture, cells were incubated in 10% AlamarBlue/DMEM solution in a humidified atmosphere at 37 °C and 5% CO_2. After 4 h, 100 mL of incubation media was transferred to 96-well plates and measured at 590 and 630 nm in order to determine the percentage of AlamarBlue reduction.

***In Vivo* Implantation on Skull of NMRI-Nude Mice.** The surgical procedure involved removal of the hair over the head *via* shaving and cleaning. The mice were anesthetized with isofluorane gas and animals were placed on ventral decubitus on a heating table, with strict aseptic conditions after skin incision, two bony defects were performed using an electrical drill with a sterile round bur under irrigation of sterile normal saline before deposition of the two same membranes and sutures with Ethicon 9/0. The skin was closed with sutures and the animal's behavior observed after waking up.

Nanoindentation. Elastic modulus and hardness of bones and different membranes in the retrieved implants were evaluated using nanoindendation. The retrieved implants (membranes attached on the bone skull), were cleaned by removing the attached tissues. The tests were carried out on the samples hydrated in formalin. In order to prepare the sample surface for nanoindentation experiments, implants were gently polished using wet cloth without any abrasive particles. Hysitron Triboindenter TI 900 with a Berkovich probe of 100 nm radius was used for the indentations. A displacement-controlled indentation cycle was applied with a maximum displacement of 100 nm at the loading/unloading rate of 10 nm s^{-1}. A dwell of 3 s was included at the maximum displacement. A total of 10−15 indents were performed on each sample. The Oliver and Pharr method was used to compute the elastic modulus.[40]

Immunofluorescence. Cells were fixed with 4% PFA over 1 h, permeabilized with 0.1% Triton X-100 for 1 h and incubated for 20 min with Alexa Fluor 546-conjugated phalloidin (Molecular Probes) for F-actin labeling and 5 min with 200 nM DAPI (Sigma) for nuclear staining. Cells were mounted on microscope slides using Vectashield (Vector) and imaged by confocal microscopy (Zeiss, LSM 510).

Confocal Laser Scanning Microscopy (CLSM). CLSM observations were documented with a Zeiss LSM 510 microscope using a ×40/1.4 oil immersion objective at 0.4 μm *z*-section intervals. FITC fluorescence was detected after excitation at 488 nm with a cutoff dichroic mirror 488 nm and an emission band-pass filter 505−530 nm (green).

Statistical Analysis. All values are expressed as mean ± SEM, and all experiments were repeated at least three times. Statistical analysis was performed using the Mann−Whitney U test. A probability p value <0.05 was considered significant to reject the null hypothesis.

Acknowledgment. This work was supported by AAP 2011 "Maturation de projets innovants" Conectus and "Alsace contre le Cancer". C.M. thanks the Faculté de Chirurgie Dentaire of Strasbourg for financial support. N.J. is indebted to CHU de Nancy, Hôpital Central, "Chirurgie Orthopédique et Traumatologie" (Contrat d'interface INSERM vers l'hôpital). G.L. thanks the "Communauté d'Agglomération d'Évreux" and the "Conseil Général de l'Eure" for partial financial support of La2B. N.J. is also indebted to Antony Rutt (starting team member of our Start Up project "ARTIOS NanoMed") for his help.

REFERENCES AND NOTES

1. Peppas, N. A.; Langer, R. New Challenges in Biomaterials. *Science* **1994**, *263*, 1715–1720.
2. Hubbell, J. A. Biomaterials in Tissue Engineering. *Biotechnology* **1995**, *13*, 565–576.
3. Langer, R.; Tirrell, D. A. Designing Materials for Biology and Medicine. *Nature* **2004**, *428*, 487–492.
4. Yang, C.; Hillas, P. J.; Báez, J. A.; Nokelainen, M.; Balan, J.; Tang, J.; Spiro, R.; Polarek, J. W. The Application of Recombinant Human Collagen in Tissue Engineering. *BioDrugs* **2004**, *18*, 103–119.
5. Griffith, L. G.; Naughton, G. Tissue Engineering—Current Challenges and Expanding Opportunities. *Science* **2002**, *295*, 1009–1014.
6. Dvir, T.; Tinko, B. P.; Kohane, D. S.; Langer, R. Nanotechnological Strategies for Engineering Complex Tissues. *Nat. Nanotechnol.* **2011**, *6*, 13–22.
7. Tang, Z.; Wang, Y.; Podsiadlo, P.; Kotov, N. A. Biomedical Applications of Layer-by-Layer Assembly: From Biomimetics to Tissue Engineering. *Adv. Mater.* **2006**, *18*, 3203–3224.
8. Cuddihy, M. J.; Kotov, N. A. Poly(Lactic-*co*-glycolic acid) Bone Scaffolds with Inverted Colloidal Crystal Geometry. *Tissue Eng. Part A.* **2008**, *14*, 1639–1649.
9. Lee, J.; Cuddihy, M. J.; Kotov, N. A. Three-Dimensional Cell Culture Matrices: State of the Art. *Tissue Eng. Part B Rev.* **2008**, *14*, 61–86.
10. Gomoll, A. H.; Madry, H.; Knutsen, G.; van Dijk, N.; Seil, R.; Brittberg, M.; Kon, E. The Subchondral Bone in Articular Cartilage Repair: Current Problems in the Surgical Management. *Knee Surg. Sports Traumatol. Arthrosc.* **2010**, *18*, 434–447.
11. Kreuz, P. C.; Steinwachs, M. R.; Erggelet, C.; Krause, S. J.; Konrad, G.; Uhl, M.; Südkamp, N. Results after Microfracture of Full-Thickness Chondral Defects in Different Compartments in the Knee. *Osteoarthritis Cartilage* **2006**, *14*, 1119–1125.
12. Oberpenning, F.; Meng, J.; Yoo, J. J.; Atala, A. *De Novo* Reconstitution of a Functional Mammalian Urinary Bladder by Tissue Engineering. *Nat. Biotechnol.* **1999**, *17*, 149–155.
13. Park, K. I.; Teng, Y. D.; Snyder, E. Y. The Injured Brain Interacts Reciprocally with Neural Stem Cells Supported by Scaffolds to Reconstitute Lost Tissue. *Nat. Biotechnol.* **2002**, *20*, 1111–1117.
14. Zhang, S. Fabrication of Novel Biomaterials through Molecular Self-Assembly. *Nat. Biotechnol.* **2003**, *21*, 1171–1178.
15. Lynn, D. M. Layers of Opportunity: Nanostructured Polymer Assemblies for the Delivery of Macromolecular Therapeutics. *Soft Matter* **2006**, *2*, 269–273.
16. Decher, G. Fuzzy Nanoassemblies: Toward Layered Polymeric Multicomposites. *Science* **1997**, *277*, 1232–1237.
17. Jessel, N.; Atalar, F.; Lavalle, P.; Mutterer, J.; Decher, G.; Schaaf, P.; Voegel, J. C.; Ogier, J. Bioactive Coatings Based on a Polyelectrolyte Multilayer Architecture Functionalized by Embedded Proteins. *Adv. Mater.* **2003**, *15*, 692–695.
18. Benkirane-Jessel, N.; Lavalle, P.; Meyer, F.; Audouin, F.; Frisch, B.; Schaaf, P.; Ogier, J.; Decher, G.; Voegel, J. C.

Control of Monocyte Morphology on and Response to Model Surfaces for Implants Equipped with Anti-inflammatory Agents. *Adv. Mater.* **2004**, *16*, 1507–1514.
19. Benkirane-Jessel, N.; Schwinté, P.; Falvey, P.; Darcy, R.; Haïkel, Y.; Schaaf, P.; Voegel, J. C.; Ogier, J. Buildup of Polypeptide Multilayer Coatings with Anti-inflammatory Properties Based on the Embedding of Piroxicam–Cyclodextrin Complexes. *Adv. Funct. Mater.* **2004**, *14*, 174–182.
20. Jessel, N.; Oulad-Abdelghani, M.; Meyer, F.; Lavalle, P.; Haïkel, Y.; Schaaf, P.; Voegel, J. C. Multiple and Time-Scheduled *in Situ* DNA Delivery Mediated by Beta-Cyclodextrin Embedded in a Polyelectrolyte Multilayer. *Proc. Natl. Acad. Sci. U.S.A.* **2006**, *103*, 8618–8621.
21. Kim, B. S.; Park, S. W.; Hammond, P. T. Hydrogen-Bonding Layer-by-Layer-Assembled Biodegradable Polymeric Micelles as Drug Delivery Vehicles from Surfaces. *ACS Nano* **2008**, *2*, 386–392.
22. Benkirane-Jessel, N.; Lavalle, P.; Hübsch, E.; Holl, V.; Senger, B.; Haïkel, Y.; Voegel, J. C.; Ogier, J.; Schaaf, P. Short-Time Tuning of the Biological Activity of Functionalized Polyelectrolyte Multilayers. *Adv. Funct. Mater.* **2005**, *15*, 648–654.
23. Dierich, A.; Le Guen, E.; Messaddeq, N.; Stoltz, J. F.; Netter, P.; Schaaf, P.; Voegel, J. C.; Benkirane-Jessel, N. Bone Formation Mediated by Synergy-Acting Growth Factors Embedded in a Polyelectrolyte Multilayer Film. *Adv. Mater.* **2007**, *19*, 693–697.
24. Facca, S.; Cortez, C.; Mendoza-Palomares, C.; Messadeq, N.; Dierich, A.; Johnston, A. P. R; Mainard, D.; Voegel, J. C.; Caruso, F.; Benkirane-Jessel, N. Active Multilayered Capsules for *in Vivo* Bone Formation. *Proc. Natl. Acad. Sci. U.S.A.* **2010**, *107*, 3406–3411.
25. Krogman, K. C.; Lowery, J. L.; Zacharia, N. S.; Rutledge, G. C.; Hammond, P. T. Spraying Asymmetry into Functional Membranes Layer-by-Layer. *Nat. Mater.* **2009**, *8*, 512–518.
26. Ding, B.; Kim, J.; Kimura, E.; Shiratori, S. Layer-by-Layer Structured Films of TiO_2 Nanoparticles and Poly(acrylic acid) on Electrospun Nanofibres. *Nanotechnology* **2004**, *15*, 913–917.
27. Müller, K.; Quinn, J. F.; Johnston, A. P. R; Becker, M.; Greiner, A.; Caruso, F. Polyelectrolyte Functionalization of Electrospun Fibers. *Chem. Mater.* **2006**, *18*, 2397–2403.
28. Ogawa, T.; Ding, B.; Sone, Y.; Shiratori, S. Super-Hydrophobic Surfaces of Layer-by-Layer Structured Film-Coated Electrospun Nanofibrous Membranes. *Nanotechnology* **2007**, *18*, 165607.
29. Lee, J. A.; Krogman, K. C.; Ma, M.; Hill, R. M.; Hammond, P. T.; Rutledge, G. C. Highly Reactive Multilayer-Assembled TiO_2 Coating on Electrospun Polymer Nanofibers. *Adv. Mater.* **2009**, *21*, 1252–1256.
30. Barnes, C. P.; Sell, S. A.; Boland, E. D.; Simpson, D. G.; Bowlin, G. L. Nanofiber Technology: Designing the Next Generation of Tissue Engineering Scaffolds. *Adv. Drug Delivery Rev.* **2007**, *59*, 1413–1433.
31. Yoo, H. S.; Kim, T. G.; Park, T. G. Surface-Functionalized Electrospun Nanofibers for Tissue Engineering and Drug Delivery. *Adv. Drug Delivery Rev.* **2009**, *61*, 1033–1042.
32. Fioretti, F.; Mendoza-Palomares, C.; Helms, M.; Al Alam, D.; Richert, L.; Arntz, Y.; Rinckenbach, S.; Garnier, F.; Haïkel, Y.; Gangloff, S. C.; Benkirane-Jessel, N. Nanostructured Assemblies for Dental Application. *ACS Nano* **2010**, *22*, 3277–3287.
33. Kenawy, E. R.; Layman, J. M.; Watkins, J. R.; Bowlin, G. L.; Matthews, J. A.; Simpson, D. G.; Wnek, G. E. Electrospinning of Poly(ethylene-*co*-vinyl alcohol) Fibers. *Biomaterials* **2003**, *24*, 907–913.
34. Sauerbrey, G. Use of Vibrating Quartz for Thin Film Weighing and Microweighing. *Z. Phys.* **1959**, *155*, 206–222.
35. Abdelkebir, K.; Gaudière, F.; Morin-Grognet, S.; Coquerel, G.; Labat, B.; Atmani, H.; Ladam, G. Evidence of Different Growth Regimes Coexisting within Biomimetic Layer-by-Layer Films. *Soft Matter* **2011**, *7*, 9197–9205.
36. Taddei, P.; Tinti, A.; Reggiani, M.; Fagnano, C. *In Vitro* Mineralization of Bioresorbable Poly(ε-caprolactone)/Apatite Composites for Bone Tissue Engineering: A Vibrational and Thermal Investigation. *J. Mol. Struct.* **2005**, *744–747*, 135–143.
37. Fowler, B. O.; Markovic, M.; Brown, E. W. Octacalcium, Phosphate. 3. Infrared and Raman Vibrational Spectra. *Chem. Mater.* **1993**, *5*, 1417–1423.
38. Crane, N. J.; Popescu, V.; Morris, M. D.; Steenhuis, P.; Ignelzi, M. A. Raman Spectroscopic Evidence for Octacalcium Phosphate and Other Transient Mineral Species Deposited during Intramembranous Mineralization. *Bone* **2006**, *39*, 434–442.
39. Voinova, M. V.; Rodahl, M.; Jonson, M.; Kasemo, B. Viscoelastic Acoustic Response of Layered Polymer Films at Fluid–Solid Interfaces: Continuum Mechanics Approach. *Phys. Scr.* **1999**, *59*, 391–396.
40. Oliver, W. C.; Pharr, G. M. An Improved Technique for Determining Hardness and Elastic Modulus Using Load and Displacement Sensing Indentation Experiments. *J. Mater. Res.* **1992**, *7*, 1564–1583.